Cation substitution effects on structural, electronic and optical properties of nonlinear optical

AgGa(S$_x$Se$_{1-x}$)$_2$ crystals

Cation substitution effects on structural, electronic and optical properties of nonlinear optical AgGa(S_xSe$_{1−x}$)$_2$ crystals

L C Tang[1]**, M H Lee**[2]**, C H Yang**[2]**, J Y Huang**[1] **and C S Chang**[1,3]

[1] Institute of Electro-Optical Engineering, National Chiao Tung University Hsinchu 305, Taiwan, Republic of China
[2] Department of Physics, Tamkang University Taipei 251, Taiwan, Republic of China

E-mail: cschang@cc.nctu.edu.tw

Abstract

The structural, electronic and optical properties of tetragonal nonlinear optical (NLO) crystals, AgGa(S_xSe$_{1−x}$)$_2$ ($x = 0.0$, 0.25, 0.5, 0.75, and 1.0), were investigated theoretically and experimentally. The results obtained indicated that the electronic bandgaps, optical properties and bulk moduli of these compounds were linearly dependent on the substitution concentration of cations. From partial density of state analysis, it was found that the electronic states near the band edges of AgGa(S_xSe$_{1−x}$)$_2$ were a simple proportional mixture of the atomic orbitals of sulfur and selenium. A cell-volume effect was proposed as the major cause of the linear dependence of material properties on the substitution concentration. It was calculated that the second-order NLO susceptibilities were scaled with the cubic power of bandgap, although a minor deviation existed. This deviation arose from the optical transition moment products.

1. Introduction

The most important technique to generate tunable coherent radiation in the mid-infrared spectrum is based on the second-order nonlinear optical (NLO) processes in a noncentrosymmetric crystal. These NLO processes include difference-frequency mixing, optical parametric generation and amplification.

The crystals used for mid-IR generation with frequency down conversion schemes should possess a wide optical transparency range from 1 μm to well beyond 5 μm. Currently those crystals are very limited and only a few of them have really become commercially available [1]. Among those available crystals, AgGaS$_2$ and AgGaSe$_2$ are well known for their

---

[3] Author to whom any correspondence should be addressed.
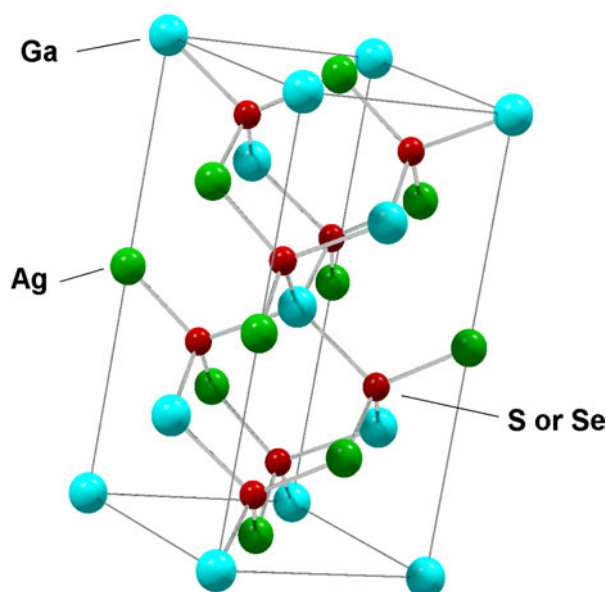
Figure 1. The crystal structure of tetragonal chalcopyrite.
(This figure is in colour only in the electronic version)

wide transparency, large birefringence, high optical damage threshold and nonlinearity. To meet the demand from specific applications, the linear and NLO properties of $AgGa(S_xSe_{1-x})_2$ can be adjusted by varying the alloy composition [2–4]. Xue *et al* [5] proposed the similar concept that most of the properties of the materials were closely correlated to the micro-structure, which depends on the constituent atoms or ions or, more precisely, the average atomic number of the constituent atoms or ions. Xue *et al* [6] also applied this concept to some I–III–VI$_2$ chalcopyrites, e.g. AgGaS$_2$ and AgGaSe$_2$, to analyse the linear and nonlinear dielectric response of these semiconductors. Other than the work of Xue *et al*, there was little on the solid solution of these ternary and quaternary chalcogenides [4, 7–11].

In this paper, the first-principles calculation of electronic structures, and optical and bulk properties of tetragonal NLO crystals, $AgGa(S_xSe_{1-x})_2$ ($x = 0.0, 0.25, 0.5, 0.75$, and 1.0), are presented. Tang *et al* used the same approach to investigate the electronic structures, and optical and bulk properties of the rhombohedral ternary halides [12] and the orthorhombic ternary nitrides [13]. The analysis with band-by-band and atomic species projection techniques [12, 13] yielded useful information about material properties and provided deep insight into the fundamental understanding of the electronic structures and optical properties of tetragonal NLO crystals, $AgGa(S_xSe_{1-x})_2$.

The synthesis method of single crystals and measurements of the optical properties in each composition are reported. Nonlinear coefficients of $AgGa(S_xSe_{1-x})_2$ were also carried out to reveal the potential of these crystals in NLO applications. The calculations were then compared with the experimental data and values in the literature.

2. Methods of simulation and experimental measurements

The crystal structure of the tetragonal chalcopyrite, AgGaS$_2$ or AgGaSe$_2$, is shown in figure 1.

The unit cell exhibits $I\bar{4}2d$ symmetry ($a = b \neq c, \alpha = \beta = \gamma = 90°$) [14, 15], which can be considered as a superstructure of two zinc blende structures. There were four metal atoms Ag, Ga, and eight crystallographically equivalent S or Se atoms in a unit cell which occupied the symmetrical positions of [(x, y, z); $(\bar{x}, \bar{y}, \bar{z})$; $(y, \bar{x}, \bar{z})$; $(\bar{y}, x, \bar{z})$; $(\bar{x} + 1/2, y, \bar{z} + 3/4)$; $(x + 1/2, \bar{y}, \bar{z} + 3/4)$; $(\bar{y} + 1/2, \bar{x}, z + 3/4)$; $(y + 1/2, x, z + 3/4)$]. In AgGa(S$_x$Se$_{1-x}$)$_2$ crystals, metal atoms are tetrahedrally coordinated by S or Se and vice versa.

2.1. First-principles calculations

The first-principles calculations were performed using a plane-wave pseudopotential approach within the framework of density-functional theory (DFT) implemented in CASTEP software [16]. The supercell (SC) of AgGaS$_2$ was assembled by enlarging the a-direction and b-direction twice ($2 \times 2 \times 1$), and then by substituting fractionally ($x = 0.00, 0.25, 0.5, 0.75$, and 1.0) atom by atom. The summation over the Brillouin zone (BZ) was carried out with a special k-point sampling using a Monkhorst-Pack grid [17]. A kinetic energy cut-off of 580 eV, 4-k special points and 96 bands were used to ensure convergence in the calculation of the optical properties.

In order to save computation time, the special k-point set was reduced to 8-k points ($3 \times 3 \times 3$ mesh) for the calculation of the equilibrium lattice constants and mechanical properties. The smaller set of k-points was found to give less than 2% difference in the equilibrium lattice constants. For comparison, a non-SC model ($1 \times 1 \times 1$) was also built up (hereafter named the single unit cell (SUC) model) with the same fractional substitution. It performed similar calculations to those with the SC models. In the *ab initio* calculation, both the 3-electron shallow-core pseudopotential in the SC model and the 13-electron shallow-core pseudopotential in SUC model for the gallium series were chosen to take into account the noticeable hybridization between the (3)d-shell and (4)p-shell electrons [18–20].

2.1.1. Calculating structural properties. The equilibrium lattice constants and fractional atomic coordinates were deduced from the total-energy minimization. Relaxation of the lattice parameters and atomic positions was carried out under the constraint of the unit-cell space-group symmetry. Energy–volume relations were obtained by varying unit-cell volume and the fitted results were obtained using the Murnaghan equation of state [21]

$$E_{\text{tot}} = \frac{B_0 V}{B_0'} \left[\left(\frac{V_0}{V} \right)^{B_0'} \left(\frac{1}{B_0' - 1} \right) + 1 \right] + E_0. \tag{1}$$

From the fitted results, the estimate of the static bulk modulus B_0 at zero pressure, and the first-order pressure derivative of the bulk modulus B_0' were obtained. The chalcopyrite structure showed two types of distortion, namely, tetragonal ($\eta = c/2a \neq 1$) and tetrahedral (internal parameter u), with respect to the zinc blende cubic structure [22–24]. The parameter u can be used to yield a measure of bond length mismatch, through the relation

$$(u - 0.25)^2 \cdot a^2 = d_{\text{AC}}^2 - d_{\text{BC}}^2 \tag{2}$$

where the subscripts A = Ag, B = Ga, and C = S or Se.

2.1.2. Electronic properties. The obtained lattice parameters were used to calculate the electronic properties of AgGa(S$_x$Se$_{1-x}$)$_2$ by proportionally substituting S and Se into the SC and the SUC model. In order to understand the nature of optical transitions and other relevant effects on the calculated optical properties, an analysis of the local densities of states (LDOS) and other electronic properties of these AgGa(S$_x$Se$_{1-x}$)$_2$ crystals was made.

Let $\Psi_{nk}(\vec{r})$ be the self-consistent wavefunction of the crystal at the nth band and kth point in the BZ, then $\Psi_{nk}(\vec{r})$ can be decomposed into a linear combination of the atomic orbitals $\Phi_{lm}^{(i)}(\vec{r})$ of each ith atom by

$$\Psi_{nk}(\vec{r}) = \sum_{i\in(\text{atoms})} \sum_{l} \sum_{m=-l}^{m=+l} C_{nk,lm}^{(i)} \Phi_{lm}^{(i)}(\vec{r}) \tag{3}$$

where $C_{nk,lm}^{(i)} = \int_{V_0} \Psi_{nk}(\vec{r}) \cdot \Phi_{lm}^{(i)*}(\vec{r}) \, dV$. The lth orbital of the α-species contributes to $\Psi_{nk}(\vec{r})$ by a fraction of $h_{nk,l}^{(\alpha)}$ [25]

$$h_{nk,l}^{(\alpha)} = \sum_{i\in(\alpha)} \sum_{m=-l}^{m=+l} C_{nk,lm}^{(i)} C_{nk,lm}^{(i)*} \bigg/ \sum_{i\in(\alpha,\beta,\gamma,\ldots)} \sum_{l} \sum_{m=-l}^{m=+l} C_{nk,lm}^{(i)} C_{nk,lm}^{(i)*}. \tag{4}$$

By using the plane-wave basis set in a plane-wave pseudopotential scheme, the representation of natural atomic orbitals around the centres of atoms was neglected. However, this disadvantage could be overcome by projecting the solved Bloch states onto the atomic orbitals constructed using the radial pseudo-atomic wavefunctions of each angular momentum channel for each element (the angular parts were simply spherical harmonic functions) [26, 27]. This was useful for extracting the local (atomic) information of the materials. Those radial pseudo-atomic wavefunctions were the ones used to generate pseudopotentials and, therefore, had the best consistency with the solved Bloch states. The projected values were equivalent to the coefficients of a linear combination of atomic orbitals (LCAO) type expansion of the original Bloch states using pseudo-atomic orbitals as basis functions. The collection of those coefficients allows local information to be extracted from the system as a whole, whereas in the present work partial or projected density of states (PDOS) plots have been used as an analysis tool. This atomic projection concept was then employed for resolving interesting components from total density of states (TDOS)

$$\text{LDOS}(\alpha, E) = \sum_{n} \sum_{k} \sum_{l} h_{nk,l}^{(\alpha)} \delta(E - E_{nk}) \tag{5}$$

$$\text{PDOS}(\alpha, l, E) = \sum_{n} \sum_{k} h_{nk,l}^{(\alpha)} \delta(E - E_{nk}). \tag{6}$$

The PDOS and LDOS could be used to provide a valuable insight into the formation of energy bandgaps and the nature of transitions from which the linear and NLO properties originated.

2.1.3. Nonlinear optical properties. For the second-order NLO response, the theoretical description was very complex [28]. However, at the zero frequency limits, the NLO susceptibility could be expressed as

$$\chi_{ijk}^{(2)}(0) = \frac{1}{V}\left(\frac{e\hbar}{m}\right)^3 \sum_{k} \sum_{vc}\left[\sum_{c'} \frac{1}{E_{c'c}E_{cv}^2 E_{c'v}^2}(D_{vc'c}^{ijk} + D_{cvc'}^{ijk} + D_{c'cv}^{ijk})\right.$$
$$\left. - \sum_{v'} \frac{1}{E_{vv'}E_{cv}^2 E_{c'v}^2}(D_{v'cv}^{ijk} + D_{vv'c}^{ijk} + D_{cvv'}^{ijk})\right] \tag{7}$$

where $D_{nml}^{ijk} = Im[p_{nm}^i(p_{ml}^j p_{ln}^k + p_{ml}^k p_{ln}^j)]/2$. Here $p_{cv}^i(k, \text{Å}^{-1})$ denotes the momentum matrix element (MME) from the conduction band c to the valence band v at the k-point of the BZ. These material properties were calculated using both the SC and the SUC model of $\text{AgGa}(\text{S}_x\text{Se}_{1-x})_2$. In section 3 the calculated and the experimental results will be compared and discussed.
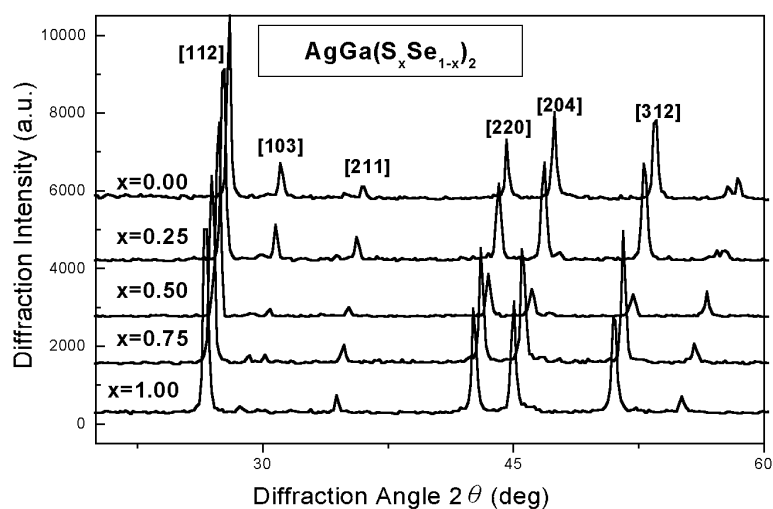
Figure 2. X-ray powder diffraction of the NLO crystals AgGa(S$_x$Se$_{1-x}$)$_2$. It can be seen that the XRD peaks shift with S composition. A minimum peak height at [312] occurs with $x = 0.5$.

2.2. Single crystal growth and measurements of the characteristics of AgGa(S/$_x$Se$_{1-x}$)$_2$

2.2.1. Single crystal growth and x-ray diffraction. The AgGa(S$_x$Se$_{1-x}$)$_2$ single crystals were grown with the vertical Bridgman technique. All the starting reagents, Ag, Ga, S and/or Se, had a nominal purity of 99.999%. Particular attention was paid to the mole ratio among the starting reagents. Since vapour compositions and partial pressures of the gaseous species were unknown, the optimum conditions for growing high quality crystals were empirically discovered. X-ray diffraction (XRD) measurement was employed to determine the lattice parameters of all the crystals AgGa(S$_x$Se$_{1-x}$)$_2$. In addition, the crystals of certain orientation relative to crystallographic axes were cut into pellets and polished on both sides for optical measurements.

2.2.2. Optical transmission measurements. The polished sample plates were loaded into a liquid-nitrogen-cooled vacuum cryostat. Optical transmission spectra were recorded from visible to mid-IR in order to determine the optical absorption edges. Then, the photoluminescence (PL) spectra were measured. The measurements of both absorption edges and PL spectra gave information about the bandgap energy E_g. These measurement were compared with the calculated results from section 2.1.2.

Fourier-transform infrared (FTIR) spectra of the AgGa(S$_x$Se$_{1-x}$)$_2$ crystals were measured from 0.8 to 18 μm to examine the transparency of these crystals.

3. Results and discussion

The calculated and measured lattice properties of five crystals are summarized in tables 1 and 2. The powder XRD patterns of AgGa(S$_x$Se$_{1-x}$)$_2$ crystals are shown in figure 2.

3.1. Crystal structure and mechanical properties

The calculated structural parameters shown in tables 1 and 2 were in good agreement with the experimental values of AgGaSe$_2$ as reported by Jaffe and Zunger [23, 24] and this work. The slight underestimation of the lattice constants was attributed to the intrinsic nature of DFT.

Table 1. Structural parameters, bond lengths and bulk moduli of the NLO crystals AgGa($S_x Se_{1-x}$)$_2$. Values from first-principles calculations for the SC model compared with the experimental values.

	x				
	0.00	0.25	0.50	0.75	1.00
a (Å) (exp.)	5.97	5.92	5.86	5.80	5.74
a (Å) (calc.)	5.87	5.89	5.77	5.66	5.63
c (Å) (exp.)	10.88	10.73	10.57	10.42	10.26
c (Å) (calc.)	10.64	10.60	10.24	10.09	10.02
Ga–S (Å) (calc.)		2.17	2.14	2.14	2.15
Ga–Se (Å) (calc.)	2.30	2.29	2.27	2.26	
Ag–S (Å) (calc.)		2.64	2.60	2.59	2.59
Ag–Se (Å) (calc.)	2.70	2.68	2.67	2.65	
η (exp.)	1.79	1.80	1.80	1.81	1.82
η (calc.)	1.81	1.87	1.84	1.85	1.84
u [S] (calc.)		0.32	0.32	0.32	0.32
u [Se] (calc.)	0.31	0.31	0.31	0.31	
B_0 (GPa) (calc.)	7.31	7.71	8.15	8.64	9.11

Table 2. The calculated structural parameters and bond lengths of the NLO crystals AgGa($S_x Se_{1-x}$)$_2$ using first-principles calculations for the SUC model.

	x				
	0.00	0.25	0.50	0.75	1.00
a (Å)	5.87	5.89	5.81	5.73	5.63
c (Å)	10.78	10.32	10.25	10.15	10.17
Ga–S (Å)		2.34	2.30	2.29	2.31
Ga–Se (Å)	2.44	2.43	2.41	2.40	
Ag–S (Å)		2.61	2.57	2.55	2.58
Ag–Se (Å)	2.67	2.65	2.63	2.65	
η	1.81	1.79	1.78	1.75	1.84
u [S]		0.29	0.29	0.29	0.29
u [Se]	0.28	0.28	0.28	0.29	

It was noted that the tetrahedral coordination of S and/or Se atoms could be distorted by the presence of two types of metal–S and/or metal–Se bonds. The average bond lengths were calculated to be Ga–S (2.17–2.15 Å), Ga–Se (2.30–2.26 Å), Ag–S (2.64–2.59 Å), and Ag–Se (2.70–2.65 Å). The calculated bond lengths of Xue *et al* were Ga–S (2.235 Å) and Ag–S (2.605 Å) in AgGaS$_2$, then Ga–Se (2.416 Å) and Ag–Se (2.601 Å) in AgGaSe$_2$. Our research presented a shorter bond length for Ga–X (X = S, Se) than the results calculated by Xue *et al*. On the other hand, we have a longer bond length for Ag–X (X = S, Se) than the results calculated by Xue *et al*.

The calculated structures of AgGa($S_x Se_{1-x}$)$_2$ appeared to be more distorted than the observed structure, which was reflected in a larger value for the bond length mismatch parameter *u* (table 1). The calculated values of AgGa($S_x Se_{1-x}$)$_2$ crystals were about 0.3 in the SC models. The *u*-parameters from SC models were consistently higher than those from

SUC models (about 0.29) and the experimental values of $AgGa(S_xSe_{1-x})_2$, reported by Jaffe and Zunger (about 0.27).

From the DFT calculations, the equation-of-state parameters such as the bulk modulus and its pressure derivative were deduced, and the results are also summarized in table 1. The bulk modulus for $AgGaS_2$ was approximately 9.11 GPa. It decreased to 8.15 GPa for $AgGa(S_xSe_{1-x})_2$ and 7.31 GPa for $AgGaSe_2$.

XRD patterns from figure 2 showed that the substitution-related diffraction peaks, e.g. at the [112] plane of $2\theta \approx 26°$ or at the [312] plane of $2\theta \approx 52°$, shifted gradually with substitution composition. From the crystal models used in this study, the S and Se atoms were located between these atomic planes. The substitution of S with Se atoms caused the change of interplanar spacing. The peaks from the [312] plane were found to have a minimum peak height when S and Se are 50% occupied. The S and Se atoms randomly occupied the crystallographic sites between the [312] planes, which resulted in a reduction in this structural factor.

The lattice parameters of $AgGa(S_xSe_{1-x})_2$ crystals varied linearly with x: $a = b \cong (5.99 - 0.55x)$ Å, $c \cong (10.87 - 0.57x)$ Å. This also generated a linear dependence of the cell volume with x: $V \cong (387.88 - 54.50x)$ Å^3.

3.2. Electronic structures, density of states and optical spectrum

The calculated bandgap values for the $AgGa(S_xSe_{1-x})_2$ crystals are now presented. The calculated bandgap which varied from 1.76 to 2.43 eV was found to be proportional to the composition of S, but inversely proportional to the cell volume. The results for the bond length in section 3.1 agreed with the concept that stronger bonding between (Ag, Ga) and (S, Se) atoms leads to a shorter bond length in $AgGa(S_xSe_{1-x})_2$ crystals with increasing S (higher (x)) composition. This observed tendency of bulk modulus in section 3.1 was consistent with the trend of the weaker bonding strength (larger unit-cell volume) and the narrower bandgap.

Grown crystals up to 10 mm in diameter and 5 cm in length could be prepared routinely. All grown samples were single crystals, which exhibit various colours from yellow ($AgGaS_2$) through red $AgGa(S_xSe_{1-x})_2$ to black ($AgGaSe_2$). For comparison with the calculated electronic bandgap, the results were obtained by both absorption edges and PL spectra which gave information about the bandgap energy E_g. Figure 3 shows the absorption edge of the resulting crystals.

In figure 3, the absorption spectra measured using a single crystal $AgGa(S_xSe_{1-x})_2$ in the visible light range are shown. The absorption edge is found to increase from 1.7 to 2.64 eV with the composition of sulfur. PL spectra (figure 4) reveal a similar trend of x-dependence. From PL measurements at room temperature, the bandgap values of $AgGa(S_xSe_{1-x})_2$ crystals can be fitted to $E_{PL}(x) \cong (1.76 + 0.65x)$ eV. The experimental data taken from Matsushita *et al* [7] and this work place the calculated bandgap between the values for the SUC model and the SC model. The resulting bandgap of $AgGa(S_xSe_{1-x})_2$ can be tuned linearly in a wide spectral range by adjusting the substitution composition. Furthermore, these crystals are all direct bandgap (see figure 5) with potential applications as efficient absorber or photon emitter.

To gain further insight into the calculated optical properties, the PDOS and LDOS spectra of these crystals were calculated (see figures 6(a)–(e)).

We found that the valence band maximums (VBM) of $AgGa(S_xSe_{1-x})_2$ were mainly contributed by the (3)p-orbital of S and (4)p-orbital of Se atoms. However the roles played by S or Se atoms at the band edges cannot be distinguished. Their contribution to the TDOS is a simple weighted summation over the S and Se compositions (see figure 6(f)). The substitution effect of the S or Se in $AgGa(S_xSe_{1-x})_2$ crystals appeared from the influences of cell volume
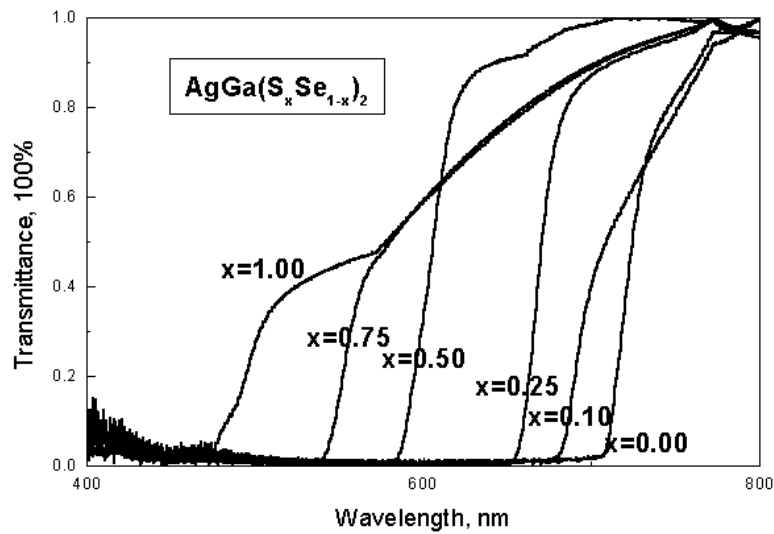
Figure 3. Absorption edge measurements of the NLO crystals AgGa(S$_x$Se$_{1-x}$)$_2$.
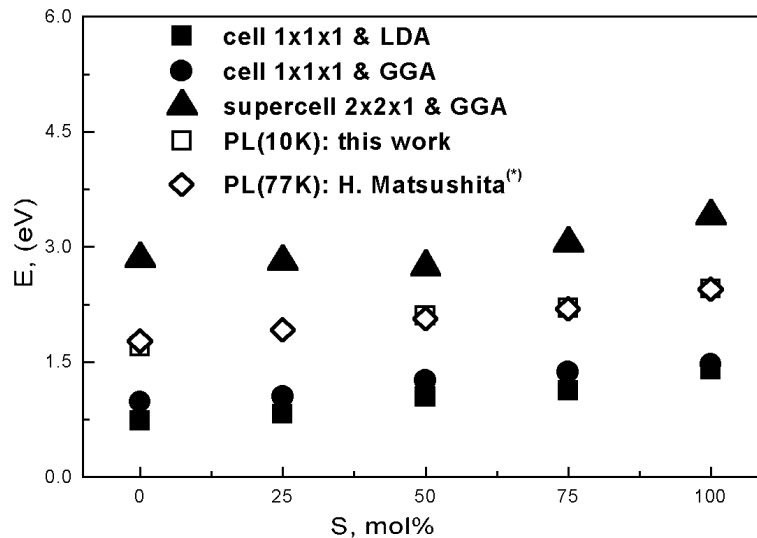
Figure 4. The first-principles calculated bandgaps and PL measurements of the NLO crystals AgGa(S$_x$Se$_{1-x}$)$_2$. (*): [7].

change. The performance of first-principles calculations on a series of artificial structures was prepared by expanding the cell volume of AgGaS$_2$ and by compressing that of AgGaSe$_2$. The calculated results showed clearly a similar effect on the bandgap and the related optical properties. This finding agreed with an empirical rule proposed by Vegard, which stated that the change of material properties caused by substitution could be calculated by simply taking a composition-weighted average of the pure substances, here AgGaS$_2$ and AgGaSe$_2$ [29–31].

FTIR measurements showed that the long wavelength limit of the transparent range of the crystals exhibited a similar dependence on substitution composition. Crystal AgGaS$_2$ had an

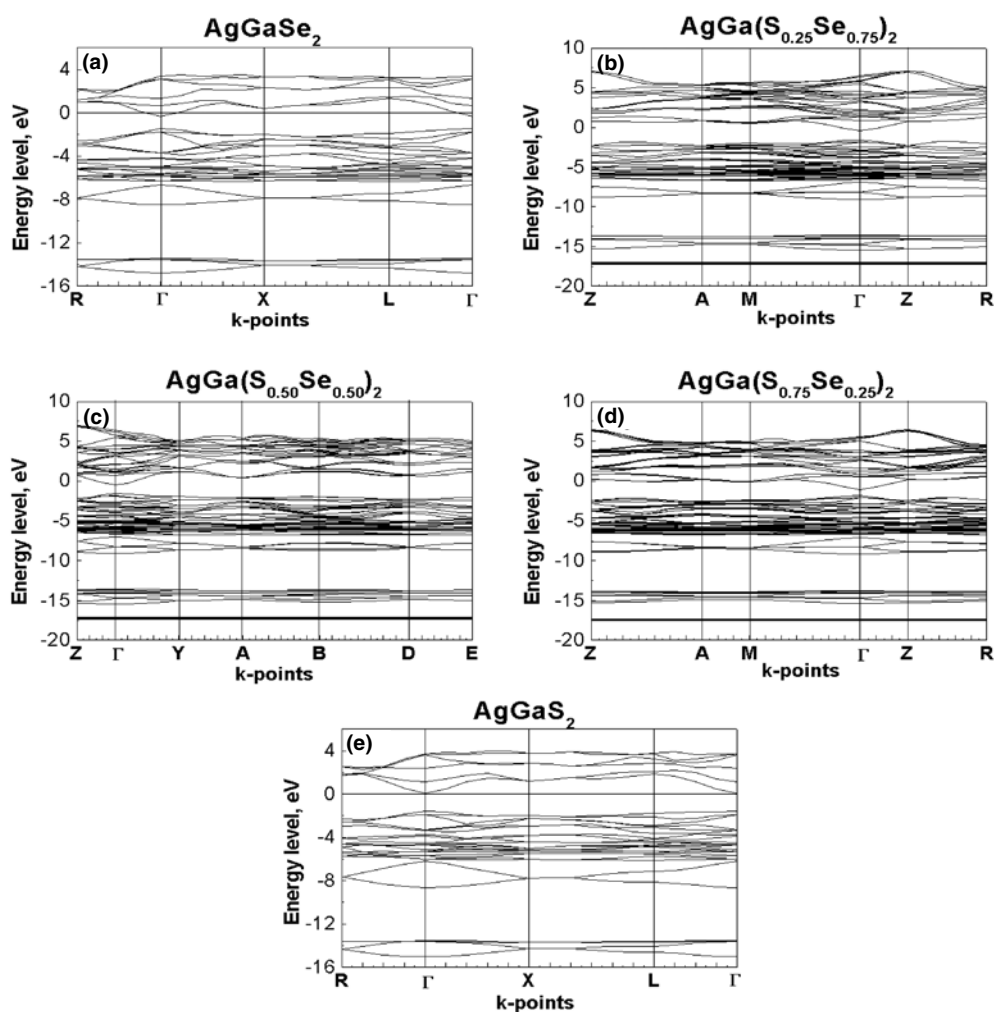**Figure 5.** Band structures of the NLO crystals AgGa(S$_x$Se$_{1-x}$)$_2$.

infrared cut-off wavelength at approximately 12 μm, which was shorter than the cut-off value of AgGaSe$_2$ (approximately 18 μm). The infrared absorption edge of AgGa(S$_x$Se$_{1-x}$)$_2$ with $x = 0.25, 0.5, 0.75$ lay approximately from 13 to 15 μm. This result was within acceptable range in view of the fact that the Se atom is heavier than S and the infrared absorption edge was dominated by the stretching modes of the S– and Se–metal bonds.

### 3.3. Second-order nonlinear optical susceptibilities

The second-order NLO susceptibility was known to be much more sensitive to crystal structure than linear optical susceptibility. The variation of the calculated second-order nonlinear susceptibilities was compared with the substitution-induced distortion. The results are summarized in the table 3. Complications from dispersion and resonant effects can be avoided by using equation (7) to calculate the static second-harmonic susceptibility (the zero frequency limit) of the AgGa(S$_x$Se$_{1-x}$)$_2$ crystals. For chalcopyrites, only two independent
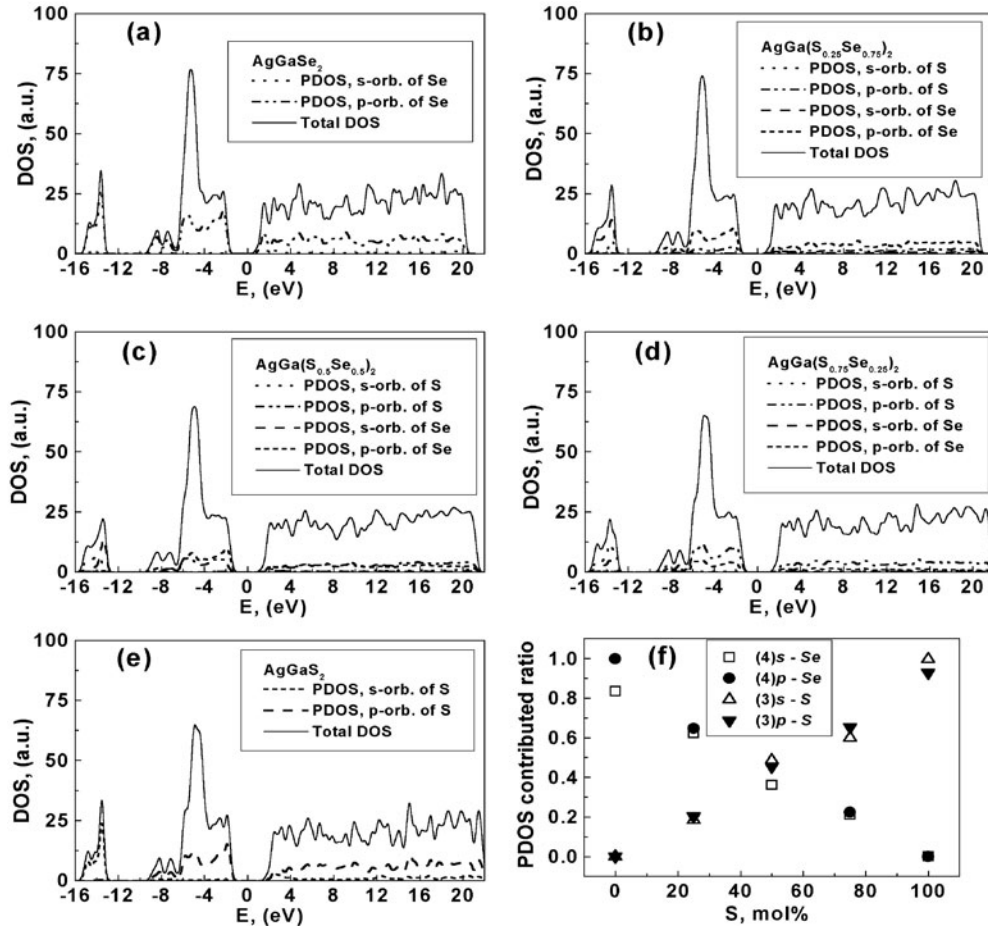
Figure 6. Analysis of the PDOS of s- and p-orbital contributions via S and Se in the NLO crystals AgGa(S_xSe$_{1-x}$)$_2$.

components, the 123 and 312 components, of $\chi^{(2)}$ exist, where 1, 2 and 3 refer to the x, y and z directions along the cubic axes respectively [32]. However, the input photon frequency being below the material absorption edge, these two components were essentially equal according to the Kleinman symmetry.

For these materials, the calculated $\chi^{(2)}_{123}$ was negative with a magnitude lying between -22.07 and -51.21 pm V^{-1} for AgGa(S_xSe$_{1-x}$)$_2$ with the SC model. The bandgap correction scheme was not utilized. These $\chi^{(2)}_{123}$ values agreed very well with the experimental results for AgGaS$_2$ and AgGaSe$_2$ [2, 6, 33–35]. Using the SUC model, the calculated $\chi^{(2)}_{123}$ ranged from -47.07 to -140.411 pm V^{-1} with different x (see table 3). These $\chi^{(2)}$ values were approximately twice as large as the values calculated using the SC model. The nonlinearity of material is inversely proportional to the cubic power of the bandgap [36]. This simple scaling rule was used to remove bandgap influence on the second-order nonlinearity. These results are presented in figure 7. AgGaS$_2$ was used as the reference and the cubic power scaling rule was employed to predict the optical nonlinearity of other crystals. The rescaled calculated $\chi^{(2)}_{123}$ using the SC model were labelled as the scaled values (filled symbols) and were compared to
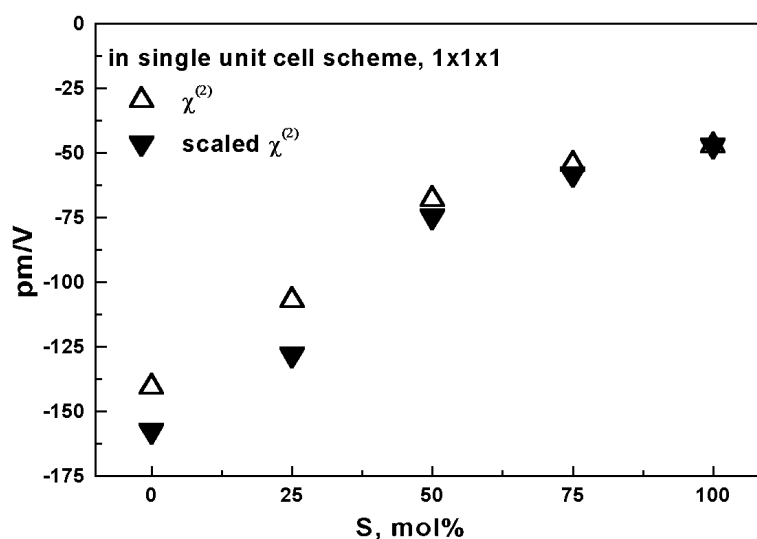
Figure 7. The first-principles calculations of the second-harmonic susceptibility $\chi^{(2)}$ and the scaled values of $\chi^{(2)}$ of the NLO crystals $AgGa(S_xSe_{1-x})_2$. The scaled $\chi^{(2)}$ values were estimated from that of the $AgGaS_2$ with a cubic power of E_g.

Table 3. The calculated $\chi^{(2)}_{123}$ (pm V^{-1}) of NLO crystals $AgGa(S_xSe_{1-x})_2$ using first-principles calculations with the SC model and the SUC model.

			x			
	0.00	0.25	0.50	0.75	1.00	Condition
This work	−51.21	−43.31	−32.14	−26.08	−22.07	SC model
Reference [6]	−42.50	—	—	—	−16.50	Bond charge model
Reference [2]	65.50	—	—	—	25.90	—
Reference [33]	64.00	—	—	—	23.00	Measured
Reference [34]	68.00	—	—	—	18.00	Measured
Reference [35]	66.00	—	—	—	22.00	Measured
This work	−140.41	−107.03	−67.90	−54.22	−47.07	SUC model

the first-principles calculations (open symbols) with the SUC model. As shown in figure 7, the deviation can be as large as 20% at $x = 0.25$. The difference was likely to originate from the transition moment products which were known to be sensitive to the detailed arrangement of the unit cell.

Based on these findings, the linearly increasing x in $AgGa(S_xSe_{1-x})_2$ caused a linear compression in cell volume, a linear increase in bandgap values and a decrease in second-order NLO susceptibility, $\chi^{(2)}$ in the cubic power of bandgap.

4. Conclusions

The structural, electronic and optical properties of tetragonal NLO crystals, $AgGa(S_xSe_{1-x})_2$ ($x = 0.0, 0.25, 0.5, 0.75$, and 1.0), have been investigated theoretically and experimentally to reveal the cation substitution effect. Based on the results, the linearly increasing x in $AgGa(S_xSe_{1-x})_2$ caused a linear compression in cell volume, a linear increase in bandgap

values and a decrease second-order NLO susceptibility. Xue *et al* discussed the linear and nonlinear dielectric responses relevant to the constituent effects. This research revealed that the NLO properties were sensitive to the electronic structures which were influenced by the unit cell structures and the constituent atoms.

The bond lengths of Ag–S, Ag–Se, Ga–S and Ga–Se were found to vary with the substitution composition, but the bond length mismatching parameter *u* did not change. It was found that the major influence of cation substitution was simply introducing a change of cell volume. PDOS analysis showed that the VBM of $AgGa(S_xSe_{1-x})_2$ were mainly contributed by the (3)p-orbital of S and (4)p-orbital of Se atoms. Their contribution to the TDOS was a simple weighted summation over S and Se compositions. The CBM and VBM were relatively shifted with the substitution concentration as well as the fundamental bandgap and, therefore, were reduced accordingly. The second-harmonic generation coefficients $\chi^{(2)}_{123}$ were also found to change with substitution. The substitution dependence could be ascribed to the bandgap change and a minor contribution from the transition moment products. Based on theoretical and experimental results obtained, these materials could be useful for both linear and NLO applications.

Acknowledgments

References

[1] Petrov V, Rotermond F and Noack F 2001 *J. Opt. A: Pure Appl. Opt.* **3** R1
[2] Rashkeev S N and Lambrecht W R L 2001 *Phys. Rev.* B **63** 165212
[3] Roberts D A 1992 *IEEE J. Quantum Electron.* **28** 2057
[4] Mikkelson J C Jr and Kidal H 1978 *J. Appl. Phys.* **49** 426
[5] Xue D, Betzler K, Hesse H and Lammers D 1999 Relationship between dielectric responses and constituent atoms in crystal materials *Phys. Status Solidi* b **216** R7
[6] Xue D, Betzler K and Hesse H 2000 Dielectric properties of I–III–VI$_2$-type chalcopyrite semiconductors *Phys. Rev.* B **62** 13546
[7] Matsushita H, Shiono O, Endo S and Irie T 1995 *Japan. J. Appl. Phys.* **34** 5546
[8] Yamamoto N, Mouri A, Seyoyama M and Horinaka H 1989 *Japan. J. Appl. Phys.* **28** 2513
[9] Balakrishnan K, Vengatesan B and Ramasamy P 1994 *J. Mater. Sci.* **29** 1879
[10] Robbins M and Lambrecht V 1973 *MRS Bull.* **8** 703
[11] Jackson A, Ohmer M and LeClair S 1997 *Infrared Phys. Technol.* **38** 233
[12] Tang L-C, Chang C-S and Huang J Y 2000 Electronic structure and optical properties of rhombohedral CsGeI$_3$ crystal *J. Phys.: Condens. Matter* **12** 9129
[13] Huang J Y, Tang L C and Lee M H 2001 *Ab initio* study of the structural and optical properties of orthorhombic ternary nitride crystals *J. Phys.: Condens. Matter* **13** 10417
[14] Abrahams S and Berstein J 1973 *J. Chem. Phys.* **59** 1625
[15] Tell B and Kasper H 1971 *Phys. Rev.* B **4** 4455
[16] Payne M C, Teter M P, Allan D C, Arias T A and DJoannopoulos J 1992 *Rev. Mod. Phys.* **64** 1045
[17] Monkhorst H J and Pack J D 1976 *Phys. Rev.* B **13** 5188
[18] Fiorentini V, Methfessel M and Scheffler M 1993 *Phys. Rev.* B **47** 13353
[19] Wright A F and Nelson J S 1994 *Phys. Rev.* B **50** 2159
[20] Karch K, Bechstedt F and Pletl T 1997 *Phys. Rev.* B **56** 3560
[21] Milman V, Lee M H and Payne M C 1994 *Phys. Rev.* B **49** 16300
[22] Camassel J, Artus L and Pascual J 1990 Lattice dynamics of AgGaSe2 i experiment *Phys. Rev.* B **41** 5717
[23] Jaffe J and Zunger A 1984 *Phys. Rev.* B **28** 5822

[24] Jaffe J and Zunger A 1984 *Phys. Rev.* B **29** 1882
[25] Sanchez-Portal D, Artacho E and Soler J M 1996 *J. Phys.: Condens. Matter* **8** 3859
[26] Segall M D, Pickard C J, Shah R and Payne M C 1996 Population analysis in plane wave electronic structure calculations *Mol. Phys.* **89** 571–7
[27] Segall M D, Shah R, Pickard C J and Payne M C 1996 Population analysis of plane-wave electronic structure calculations of bulk materials *Phys. Rev.* B **54** 16317–20
[28] Rashkeev S N, Lambrecht W R L and Segall B 1998 *Phys. Rev.* B **57** 3905
[29] Fong C and Phillips J 1976 *Phys. Rev.* B **14** 5387
[30] Wooly J, Williardson R and Goering H 1962 *Compound Semiconductors* (New York: Reinhold)
[31] Wooly J 1962 *Compound Semiconductors* (New York: Reinhold)
[32] Wyckoff R W G 1963 *Crystal Structures* (New York: Interscience)
[33] Shay J L and Wernick J H 1975 *Ternary Chalcopyrite Semiconductors: Growth, Electronic Properties, and Applications* (Oxford: Pergamon)
[34] Kurtz S K, Jerphagnon J and Choy M M 1979 *Numerical Data and Functional Relationships in Science and Technology* (Oxford: Pergamon) p 671
[35] Roberts D A 1992 *IEEE J. Quantum Electron.* **27** 142
[36] Shen Y R 2002 *The Principles of Nonlinear Optics* (New York: Wiley)